Original Article

Journal of Tissue Engineering
Volume 10: 1–16

DOI: 10.1177/2041731419845852
journals.sagepub.com/home/tej
SAGE

3D gelatin-chitosan hybrid hydrogels combined with human platelet lysate highly support human mesenchymal stem cell proliferation and osteogenic differentiation

Federica Re[1,2], Luciana Sartore[3], Vladimira Moulisova[4,5], Marco Cantini[5], Camillo Almici[6], Andrea Bianchetti[6], Clizia Chinello[7], Kamol Dey[3], Silvia Agnelli[3], Cristina Manferdini[8], Simona Bernardi[1,2], Nicola F. Lopomo[9], Emilio Sardini[9], Elisa Borsani[10,11], Luigi F. Rodella[10,11], Fabio Savoldi[12,13], Corrado Paganelli[12], Pierangelo Guizzi[14], Gina Lisignoli[8], Fulvio Magni[7], Manuel Salmeron-Sanchez[5] and Domenico Russo[1]

Abstract

Bone marrow and adipose tissue human mesenchymal stem cells were seeded in highly performing 3D gelatin–chitosan hybrid hydrogels of varying chitosan content in the presence of human platelet lysate and evaluated for their proliferation and osteogenic differentiation. Both bone marrow and adipose tissue human mesenchymal stem cells in gelatin–chitosan hybrid hydrogel 1 (chitosan content 8.1%) or gelatin–chitosan hybrid hydrogel 2 (chitosan 14.9%) showed high levels of viability (80%–90%), and their proliferation and osteogenic differentiation was significantly higher with human platelet lysate compared to fetal bovine serum, particularly in gelatin–chitosan hybrid hydrogel 1. Mineralization was detected early, after 21 days of culture, when human platelet lysate was used in the presence of osteogenic stimuli. Proteomic characterization of human platelet lysate highlighted 59 proteins mainly involved in functions related to cell adhesion, cellular repairing mechanisms, and regulation of cell differentiation. In conclusion, the

[1]Department of Clinical and Experimental Sciences, University of Brescia, Bone Marrow Transplant Unit, ASST Spedali Civili, Brescia, Italy
[2]Centro di Ricerca Emato-Oncologica AIL (CREA), ASST Spedali Civili, Brescia, Italy
[3]Department of Mechanical and Industrial Engineering, University of Brescia, Brescia, Italy
[4]Biomedical Center, Faculty of Medicine in Pilsen, Charles University, Pilsen, Czech Republic
[5]Centre for the Cellular Microenvironment, Division of Biomedical Engineering, School of Engineering, University of Glasgow, Glasgow, UK
[6]Department of Transfusion Medicine, Laboratory for Stem Cells Manipulation and Cryopreservation, ASST Spedali Civili, Brescia, Italy
[7]Department of Medicine and Surgery, Clinical Proteomics and Metabolomics Unit, University of Milano-Bicocca, Vedano al Lambro, Italy
[8]IRCCS Istituto Ortopedico Rizzoli, Laboratorio di Immunoreumatologia e Rigenerazione Tissutale, IRCCS Istituto Ortopedico Rizzoli, Bologna, Italy
[9]Department of Information Engineering, University of Brescia, Brescia, Italy
[10]Department of Clinical and Experimental Sciences, University of Brescia, Brescia, Italy
[11]Interdipartimental University Center of Research "Adaptation and Regeneration of Tissues and Organs (ARTO)," University of Brescia, Brescia, Italy
[12]Department of Orthodontics, Dental School, University of Brescia, Brescia, Italy
[13]Dental Materials Science, Discipline of Applied Oral Sciences, Faculty of Dentistry, The University of Hong Kong, Hong Kong
[14]Orthopedics and Traumatology Unit, ASST Spedali Civili, Brescia, Italy

Corresponding author:
Domenico Russo, Department of Clinical and Experimental Sciences, University of Brescia, Bone Marrow Transplant Unit, ASST Spedali Civili, Piazzale Spedali Civili 1, 25123 Brescia, Italy.
Email: domenico.russo@unibs.it

combination of our gelatin–chitosan hybrid hydrogels with hPL represents a promising strategy for bone regenerative medicine using human mesenchymal stem cells.

Keywords
Hybrid chitosan-gelatin hydrogel, human mesenchymal stem cells, human platelet lysate, tissue engineering, bone regeneration

Date received: 6 February 2019; accepted: 2 April 2019

Introduction

Regenerative medicine has been receiving growing attention as treatment approach for various tissue injuries. Current tissue engineering strategies are mainly focused on the restoration of damaged tissue by using human mesenchymal stem cells (hMSCs) either alone or in combination with three-dimensional (3D) scaffolds. In particular, to restore the bone's structural integrity, implantation of scaffolds bioengineered with hMSCs represents the most promising technique since it combines the properties of the scaffolds with the activities of MSCs.[1]

Scaffolds are generally 3D porous substrates designed to promote cell-biomaterial interactions, permitting sufficient transport of gases, nutrients, and regulatory factors for cell survival, proliferation, and differentiation. In addition, they can biodegrade with a controlled rate as the tissue regenerates, while triggering minimal degrees of inflammation or toxicity *in vivo*.[2–7]

For the purpose of our study, high-performance porous scaffolds were synthetized starting from gelatin (G), polyethylene glycol (PEG), and chitosan (CH) (G-CH hybrid hydrogels) to support hMSCs proliferation and osteogenic differentiation.

Hydrogels are 3D polymeric biomaterials that can be tuned to have properties similar to the natural extracellular matrix (ECM). Whereas naturally derived hydrogels are biocompatible, bioactive, and biodegradable and promote many cellular functions, synthetic hydrogels are highly reproducible, and characterized by high mechanical properties.[8]

G has been extensively used in the field of tissue engineering due to its biocompatibility and biodegradability.[9] Similarly, CH has several beneficial properties that make it a good candidate for biomedical applications. It is biocompatible, biodegradable, non-antigenic, non-toxic, antimicrobial, and shows haemostatic activity.[10] In addition, its structure mimicking natural ECM constituents and cationic surface charges are expected to promote cell attachment and growth.[11]

hMSCs have been demonstrated to promote tissue repair thanks to their ability to migrate to injured tissues, and their immunomodulatory and trophic effects.[12] These cells can be isolated from various tissues, mainly including bone marrow (BM), adipose tissue (AT), and cord blood (CB); can be expanded in quantities that are sufficient for potential therapeutic applications; and show self-renewal capacity and ability to differentiate *in vitro* into osteoblasts, adipocytes, and chondroblasts.[13,14]

In this study, we used both BM and AT-hMSCs within the G-CH hybrid hydrogels, in the presence of either fetal bovine serum (FBS) or human platelet lysate (hPL). hPL has been recently introduced as a substitute for FBS since it allows to avoid the risks of transmitting animal diseases and potential immune responses to animal antigens and also may overcome the strict rules of regulatory authorities in charge of the approval of experimental protocols for somatic cell therapies.[15–19] Furthermore, platelet derivatives are widely applied in different clinical fields, since they function as tissue sealant and delivery system for mitogenic and chemotactic growth factors (GFs). In doing so, cell proliferation, angiogenesis, and cell migration are stimulated, and tissue regeneration favored.[20]

Thus, in this study, we tried to establish, in vitro, a clinical grade biomedical device for potential use in bone regenerative medicine, by seeding BM-hMSCs and AT-hMSCs in G-CH hybrid hydrogels in the presence of hPL and evaluating their viability, proliferation, and osteogenic differentiation.

Materials and methods

Reagents

Type A G (pharmaceutical grade, 280 bloom, viscosity 4.30 mPs), produced from pig skin, was purchased from Italgelatine, Italy. CH (molecular weight between 50,000 and 190,000 Da and degree of deacetylation 75%–85%) was obtained from Fluka, Italy. Poly(ethylene glycol)diglycidyl ether (molecular weight 526 Da) was supplied by Sigma-Aldrich, Italy. Ethylene diamine (EDA) and acetic acid were provided by Fluka, Italy. Dulbecco's modified Eagle's medium (DMEM), L-glutamine, penicillin-streptomycin, and sodium pyruvate were purchased from Sigma-Aldrich, USA. Amphotericin B and minimum essential medium (MEM) non essential amino acids solution were purchased from Gibco, ThermoFisher Scientific, USA.

G-CH hybrid hydrogels synthesis. G-CH hydrogels were prepared in aqueous solution and the synthetic procedure

involved the reaction between G/CH amino-groups and the epoxy groups of functionalized PEG.

Briefly, G (6 g) was dissolved in 65 mL distilled water at 45°C under mild magnetic stirring followed by dropwise addition of PEG (1.4 g) and EDA (70 mg). CH solution in acetic acid (2 wt%, 33 g) were added and the final reaction mixture was gently magnetically stirred at 45°C for 20 min to obtain homogeneous mixture and then poured into the glass plate for gel formation. The gels were cut into rectangular bar or dumbbell and then were frozen by dipping into liquid nitrogen bath maintained at a temperature of –196°C. The frozen samples were freeze-dried using an Edwards Modulyo freeze-drier operating under vacuum at –60ºC, for sublimation of ice crystals. Finally, in order to further increase the degree of grafting, the dried samples were put into oven at 45°C for 2 h under vacuum. The final products obtained after freeze drying and post-curing process maintained well their size and shape. In order to obtain proper composition, two different amounts of CH were added obtaining the final dry hydrogels, namely G-CH1 (CH content 8.1%) and G-CH2 (CH content 14.9%). Hydrogels were sterilized by gamma irradiation with Cobalt 60 gamma rays using 27–33 kGy following UNI EN ISO 11137 (Sterilization of Health Care Products).

Chemical morphological and mechanical characterization of G-CH hybrid hydrogels. The texture, morphology and porous structure of hydrogels were analyzed by scanning electron microscopy (SEM) using a LEO EVO 40 scanning electron microscope. The dry samples were cryogenically fractured.

Mechanical tests were carried out by an Instron series 3366 testing machine, equipped with a 50 N load cell. Tensile tests were carried out at a cross-head rate of 10 mm/min. Specimens were cut from the sample disk into a dumbbell shape. The actual width and thickness of the specimens in the narrow portion of the dumbbell were measured using an optical traveling microscope. The samples, having a gauge length of 25 mm, were clamped at a larger distance and stretched until failure. At least six specimens were tested for each hydrogel composition. Engineering stress was calculated by dividing the recorded force by the initial cross-sectional area. Engineering strain was calculated as the ratio of cross-head displacement to initial length. Initial elastic modulus (stiffness, E) was determined from the slope of the initial linear segment of stress–strain curves. To find a precise tensile strength (σ_b), considering the significant variation of thickness of the specimen, tensile strength was taken as the maximum force divided by the minimum cross-sectional area of the specimen. The strain value corresponding to the maximum stress was considered as an elongation at break (ε_b). The specimens were tested after immersion in distilled water for 2 h at 37°C (swollen condition). For the compression test, samples were cut into cubic specimens and compressed by two parallel metal platens connected to the load cell, at a rate of 10% strain per min at room temperature (RT). The specimens were tested in wet condition. Engineering stress was calculated by dividing the recorded force by the initial cross-sectional area. Engineering strain under compression was calculated as the ratio of cross-head displacement to original length/thickness. Initial elastic modulus (stiffness, E) was determined from the slope of the initial linear segment of stress–strain curves. Cyclic loading–unloading experiments were performed for up to 10 cycles with 50% maximum strain without relaxation time in order to evaluate the reversible behavior of hydrogels. Cyclic compression tests were also performed over time (1, 10 and 21 days) to monitor the mechanical integrity of the hydrogels during hydrolytic degradation.

Hydrolytic mass loss evaluation and swelling ratio. The preweighed (W_i) samples were incubated in distilled water at 37°C over a 3-week period. At regular intervals of 1, 10, and 21 days, the samples were removed, weighed (W_w), rinsed with fresh water, air dried followed by vacuum drying at 45°C for 4 h, and finally dried mass (W_f) was measured. The swelling ratio (%) and mass loss (%) was calculated using following equations

$$\text{Swelling ratio}(\%) = \frac{(W_w - W_f)}{W_f \times 100}$$

$$\text{Mass loss}(\%) = \frac{(W_i - W_f)}{W_i \times 100}$$

hPL production. hPL for mesenchymal stem cells expansion was obtained from blood donations belonging to the Blood Bank of ASST Spedali Civili of Brescia and produced according to standardized clinical grade procedures in closed systems.[17] From the automatic separation of whole blood (CompoMat G5, Fresenius Kabi AG, Germany), fresh frozen plasma (FFP), buffy coat (BC), and red blood cells units were obtained. Within 48 h of collection, 12 (6 + 6) group 0 BC units were pooled (BioP flex Pool, Fresenius Kabi AG, Germany), each diluted in group AB FFP (250–300 mL) and gently centrifuged (340 g, 6 min, 22°C—Heraeus Cryofuge 6000i, Thermo Fisher Scientific, USA). At this point, the supernatant obtained is transferred to a satellite bag and in-line filtered for leukocytes depletion. Residual leukocyte count (<0.2/mL) was performed by flow cytometry (Kit Leucocount, Facs Canto II, Becton Dickinson, Itay). Platelet-rich plasma (PRP) obtained was transferred to a 600 mL bag (Compoflex 1 F, Fresenius Kabi AG, Germany), adjusted with FFP, at a platelet concentration of $1.0 \pm 0.2 \times 106/\mu L$ (sodium heparin 40UI/mL), frozen at −80°C for 24 h, and thawed at 37°C for 25 min (DH8 QuickThaw™, Helmer Inc., USA) to lyse platelets. After a second centrifugation (4000 g,

15 min, 22°C) aimed at removing platelet bodies or debris, the hPL obtained was aliquoted into 50 mL tubes (BD Falcon™ Conical Tubes, Becton Dickinson, Itay) and stored at −80°C until use. Sterility tests were done to prove hPL negativity for aerobic /anaerobic bacteria.

Platelet poor plasma production

Platelet-poor plasma (PPP) was produced from PRP according to standardized blood bank procedures in closed systems finally containing less than 10×10^3 platelets/μL. Four units of whole blood belonging to the Blood Bank of ASST Spedali Civili of Brescia were centrifuged (3400 g, 3 min, 22°C—Heraeus Cryofuge 6000i, Thermo Fisher Scientific, USA), so that the optimal number of platelets remained in plasma (PRP). Platelets from PRP were sedimented by hard spin centrifugation (5050 g, 6 min, 22°C); the supernatant PPP was transferred to a satellite 600 mL bag (Compoflex 1 F, Fresenius Kabi AG, Germany) and subsequently aliquoted into 50 mL tubes (BD Falcon™ Conical Tubes, Becton Dickinson, Itay) and stored at –80°C until use as reference background in GFs determination on hPL. All the blood units used for the production of hPL and PPP were biologically qualified according to Italian legislation complying with EU legislation.

hPL proteomic characterization by nLC-ESI MS/MS

Quali-quantitative evaluation of hPL compared to PPP was achieved by nLC-ESI MS/MS *shotgun* proteomics. In particular, one batch of hPL and four distinct PPP samples from different donors (n = 4) were processed and evaluated for proteomic characterization.

High abundant proteins, as albumin and IgG, were depleted from plasma-derived samples using ProteoPrep® Immunoaffinity Albumin and IgG Depletion Kit (PROTIA Depletion kit, Sigma-Aldrich, USA), following manufacturer's instructions before MS analysis protocol. Both depleted and not depleted samples were processed and analyzed in MS.

In particular, a volume corresponding to 300 μg of proteins for each sample was trypsinized based on filter aided sample preparation (FASP) strategy as previously described.[21] Digestion was performed overnight at 37°C onto ultrafiltration units (Amicon Ultra–0.5 mL 30 kDa, Millipore, USA) after reduction with 50 mM dithiothreitol and alkylation (100 mM iodoacetamide). No urea or sodium dodecyl sulfate (SDS) was added, and 50 mM ammonium bicarbonate was used as buffer in each step. About 1 μg of peptide mixtures were injected into UHPLC system (Ultimate™ 3000 RSLCnano, ThermoFisher Scientific, USA) coupled online with Impact HD™ UHR-QqToF (Bruker Daltonics, Germany) as already reported.[22,23] Technical variability for label-free relative quantification was minimized injecting each sample at least twice (for each single sample of PPP) and four times (for the sample of hLP).

Protein identities were determined using an in-house Mascot search engine (version: 2.4.1), using Swissprot reference databases of *Homo sapiens* (accessed June 2018, 557,713 sequences; 200,130,199 residues) and the following parameters: enzymatic digestion by trypsin, allowing one missed cleavage; precursor mass tolerance was set as 20 ppm; fragment mass tolerance of 0.05 Da; carbamidomethylation (Cys) as fixed modification. Decoy database and a false discovery rate (FDR) less than 1%, were applied. Only proteins with at least one unique peptide ($p \leqslant 0.05$) were considered identified.

Peaks Studio 8.5 (Bioinformatics Solutions Inc., Waterloo, ON, USA) was utilized to determine the relative abundances of identified proteins.[24] All replicates were loaded separately. The areas under the curve of the extracted ion chromatograms were measured and normalized using total ion current (TIC). As protein filter a significance of 13 (FDR with adjusted p-value of ⩽1%) was used for identification. Only peptide features having a quality ⩾2, an average area ⩾104 and a charge from 1 to 10, and only proteins that had been identified with at least two unique non redundant peptides were selected for quantitation. Analysis of variance (ANOVA) test integrated into the software was chosen to evaluate the significance of the comparison ($p < 0.05$). A fold change of 1.5 was applied and only proteins that showed significant differences in at least 4 of 12 replicates were considered. Functional annotation was performed using String Online Tool.[25,26]

Human BM and AT mesenchymal stem cells (BM-AT-hMSCs) culture

Human BM mesenchymal stem cells (BM-hMSCs) and human AT mesenchymal stem cells (AT-hMSCs) were purchased from PromoCell, Germany. BM-hMSCs and AT-hMSCs were expanded in the presence of a growth medium (GM) consisting of DMEM, a high glucose-based medium with 2% L-glutamine/penicillin-streptomycin/amphotericin B solution (stock solution, 200 mM L-glutamine, 10 000 U/mL penicillin, 10 mg/mL streptomycin, 250 μg/mL amphotericin B), 1 mM sodium pyruvate, MEM Non Essential Amino Acids Solution 1X and 10% FBS (referred as complete medium FBS) or 5% hPL (referred as complete medium hPL) at 37°C and 5% CO_2 in an incubator.

BM-AT-hMSCs cell viability and cell proliferation assay

BM-hMSCs and AT-hMSCs were detached from the flask using trypsin ethylenediaminetetraacetic acid after reaching 80% of confluence, neutralized with complete medium

FBS, centrifuged at 1100 r/min for 5 min, resuspended in the GM, and counted with a hemocytometer. A cell suspension at a cellular density of 10^6cells/mL (36×10^3cells/scaffold) was added to the scaffolds. Scaffolds with volume of approximately 36 mm^3 (approximately dimensions: 3 mm × 3 mm x 4 mm) were used. The required amount of BM-hMSCs and AT-hMSCs cells at passage 3 was added to each scaffolds by direct cell seeding in 24 uncoated multiwell plates, then incubated at 4°C for 1 h and 37°C under 5% of CO_2 conditions for 1 h. In fact, it was previously observed that this cold static seeding method improves cell penetration generating a uniform initial cell distribution in the porous scaffolds.[27] After this time, 1 mL of complete medium FBS or complete medium hPL were added to each well and cell viability was analyzed after 21 days and cell proliferation was analyzed after 2, 6, 10, 14, and 21 days.

Cells viability was evaluated using a Live/Dead kit for mammalian cells (ThermoFisher, USA). The samples were washed with Dulbecco's phosphate-buffered saline (DPBS) and incubated for 30–45 min at RT in DPBS with 2 μM of calcein AM and 4 μM of ethidium homodimer-1 (EthD-1). NucBlue® Live reagent (2 drops/mL) for nuclei staining was added to the cultures. An analysis of live (stained in green with calcein AM) and dead (stained in red with EthD-1) cells was then performed using a Zeiss Observer Z1 fluorescence microscope. Ten images were taken from three different replicates of each sample and the percentage of viable cells (% total cell number – % dead cells) was then calculated for each conditions using Image J.

Cell proliferation was determined using the Cell Counting Kit-8 (CCK-8, Sigma-Aldrich, USA) on days 2, 6, 10, 14, and 21 of cell culture, following manufacturer instructions. The formazan produced by the CCK-8 assay is shown to be proportional to the number of viable cells giving rise to a colored compound that can be measured spectrophotometrically at 450 nm. Briefly, the cell-cultured samples (three replicates) were moved to a new cell culture plate at each time points and incubated with a fresh culture medium containing the CCK-8 reagent (ratio 1:10) at 37°C for 2 h 30 min. Then, the absorbance of 100 μL of supernatant transferred to a new cell culture plate was measured at 450 nm with an Infinite 200 PRO plate reader (Tecan, Switzerland). Absorbance at 450 nm is proportional to the number of viable cells in each sample. Indeed, a standard curve was created by culturing known numbers of viable cells in order to determine the relative viable cells number proliferating in the hydrogels.

BM-AT-hMSCs osteogenic differentiation

A cell suspension at a cellular density of 10^6cells/mL (36×10^3cells/scaffold) was added to the scaffolds for osteogenic differentiation in static conditions. To induce osteogenic differentiation, cells-scaffolds constructs were cultured in 24-uncoated well plates for 3 weeks with osteogenic differentiation medium (OM), consisting of complete medium FBS or complete medium hPL supplemented with 10^{-7} M dexamethasone, 25 μg/mL L-ascorbic acid, and 3 mM NaH_2PO_4. All samples were analyzed in triplicates. As controls, samples were also cultured in the complete medium FBS or complete medium hPL without additional osteogenic factors for 3 weeks, to evaluate the osteogenic potential of the hydrogels alone.

After 21 days of culture, scaffolds were fixed with formaldehyde 4% for 1 h at 4°C. After the fixing step, the samples were soaked overnight in 30 w/v % sucrose in DPBS, embedded in OCT compound (VWR, USA, 361603E), and frozen in liquid nitrogen. Finally, 80 μm sections were cut out with a Leica CM 1860 ultraviolet (UV) cryostat. Sections were collected and placed onto Thermo Scientific superfrost ultra plus slides (J3800AMNZ). For immunostaining, sections were encircled by immunoEdge pen, rehydrated in PBS, permeabilized with 0.1 vol % Triton X-100 in PBS 1X and then blocked for non-specific binding sites by incubation with bovine serum albumin 1% in PBS (PBS-BSA 1%) for 1 h. To analyze osteogenic differentiation of cells inside the scaffolds, primary antibodies (mouse monoclonal anti-osteocalcin (OCN), Santa Cruz Biotechnologies, USA, ABOC-5021) were diluted 1:50 in PBS-BSA 1%. After 1 h of incubation at 37°C, sections were then washed in PBS and incubated with the secondary antibodies (rabbit anti-mouse Cy3, Jackson Immunoresearch, USA, 315-165-003) diluted 1:100 in PBS-BSA 1% for 1 h at RT. To analyze actin cytoskeleton of the cells in the scaffolds Alexa Fluor 488 phalloidin (Invitrogen, USA, A12379) was diluted 1:100 in PBS-BSA 1% for 30 min at RT. Finally, samples were washed three times with PBS adding 0.5% Tween-20 before mounting the coverslip with a drop of Vectashield (Vector Laboratories, USA) containing 4′,6-diamidino-2-phenylindole (DAPI) to counterstain cell nuclei (blue). Images were acquired with an inverted Zeiss Observer Z1 fluorescence microscope. The samples were analyzed in triplicates. Fluorescent intensity was analyzed using ImageJ and normalized according to the cell number.

For von Kossa staining, the sections were air-dried for 20 min and fixed in 10% formaldehyde (Kaltek, Italy) at RT for 1 h. Then, samples were rehydrated and stained with 5% aqueous silver nitrate (Sigma-Aldrich, USA) solution under UV light for 30 min, rinsed in de-ionized water, immersed in 5% sodium thiosulfate solution (Sigma-Aldrich, USA) for 5 min RT. Samples were counterstained with hematoxylin. Images were acquired using Eclipse 90i microscope (Nikon Instruments Europe BV).

SEM and element analysis

BM-hMSCs were seeded on the scaffolds at 10^6cells/mL and were fixed in paraformaldehyde 4% for 1 h at 4°C.

Table 1. Composition tensile and compressive properties of G-CH polymeric scaffolds.

Sample	Composition (%)			Tensile properties			Compressive properties	
	G	PEG	CH	E (MPa)	σb (MPa)	εb (%)	E (MPa)	σ (MPa)[a]
G-CH1	74.3	17.6	8.1	0.68 ± 0.26	0.25 ± 0.15	29 ± 4	0.25 ± 0.05	0.046 ± 0.005
G-CH2	68.8	16.3	14.9	0.28 ± 0.14	0.08 ± 0.03	26 ± 3	0.25 ± 0.05	0.065 ± 0.005

G: gelatin; PEG: polyethylene glycol; CH: chitosan.
[a]Stress at 50% strain.

Then, cells were washed 3 times in 0.1 M sodium cacodylate buffer before a 1 h incubation in 1% osmium tetroxide/0.1 M sodium cacodylate buffer. Samples were then washed three times with distilled water and stained with 0.5% uranyl acetate/distilled water for 1 h in the dark. Samples were washed again with distilled water before dehydration through an ethanol gradient (washing in 30%, 50%, 70%, and 90% ethanol 10 min per each step, and 5 min washing for 4 times in 100% ethanol). Finally, samples were loaded onto a POLARON E3000 Critical Point Dryer (Liquid CO_2) for 1 h 20 min and then given a gold/palladium coating using a POLARON SC515 SEM COATER and viewed on a JEOL6400 SEM running at 10 kV. Adhesion and morphology of BM-hMSCs were evaluated after 2 and 21 days in complete medium FBS or hPL, differentiation of BM-hMSCs was evaluated after 21 days in OM with hPL. Element analysis was done for selected samples, and SEM-related images were acquired using Philips XL30 ESEM with a ThermoFisher Ultradry EDX detector to evaluate calcium phosphate deposition after 21 days of differentiation.

Statistical analysis

For the statistical studies of the in vitro assessment of cells proliferation and osteogenic differentiation on the G-CH hydrogels, GraphPad Prism was used. One-way ANOVA with Tukey's post hoc test and two-way ANOVA with Bonferroni post hoc test were performed as specified in the captions in the Figures. Three replicates of each sample were used. Statistical significance was accepted at the probability level $p < 0.05$. Data are expressed as mean ± standard deviation.

Results

G-CH hybrid hydrogels

Two different polymeric scaffolds namely G-CH1 and G-CH2 having a CH content of 8.1% and 14.9 wt%, respectively (Table 1), were prepared using a green, simple and easy synthetic method under aqueous condition without using any solvents, chemical reagents such as catalysts, coupling or foaming agents.

Functionalized PEG was used as a crosslinking agent, and the cross-linking process involved mainly end epoxide groups of PEG and amino group of G and CH chains. The final well interconnected macroporous scaffold structures were obtained by ice segregation induced self-assembly, which consists in the freezing of the hydrogel into liquid nitrogen followed by freeze-drying. During freezing by liquid nitrogen, ice crystals formed, and they acted as templates to create the macroporous structure after freeze drying. Hydrogel morphology was analyzed by SEM.

The image of cross-sectional views reported in Figure 1(a) clearly showed a highly interconnected porous network morphology with macro and micro-porosity, channels and interstices of different size, well interconnected, and homogeneously distributed.

Results of tensile and compressive tests performed on wet specimens (Table 1) are compatible with stable high crosslinked hydrogels. The tensile modulus, tensile strength and elongation at break of the G-CH1 scaffold were found to be 0.68 MPa, 0.25 MPa and 29%, respectively. Increasing amount of CH into the G-CH network reduced stiffness (0.28 MPa) and strength (0.08 MPa), producing a softer material.

To investigate the mechanical stability and reversibility of the hydrogels, consecutive cyclic loading–unloading compressive tests with up to 50% of strain were done on wet cubic specimens and the value of elastic modulus and strength are reported in Table 1. During the first cycles, the hydrogels showed a Mullins effect, with the reduction of stiffness and stress at every cycle.[28] After few cycles, the material behavior was stabilized (Figure 1(b)) and the hydrogels were able to sustain a compressive strain of 50% with full strain recovery. Both the hydrogels maintained their original shape and their load bearing capability up to such a high level of deformation. Although many microscopic flaws might have been created within the hydrogel, no macroscopic crack propagated through the sample; these broken bridges did not lead to macroscopic fracture of the hydrogel.

Controlled degradability of materials without sacrificing their structural stability and mechanical integrity is important for long-term service of hydrogels. Degradation significantly affects structural stability, swelling ratio, and mechanical integrity.[29] Therefore, we investigated hydrogel hydrolytic degradation by measuring mass loss, swelling ratio, and mechanical stiffness/strength at predetermined time of 1, 10, and 21 days. Figure 1(c) shows the mass loss and swelling ratio as a function of degradation time over a

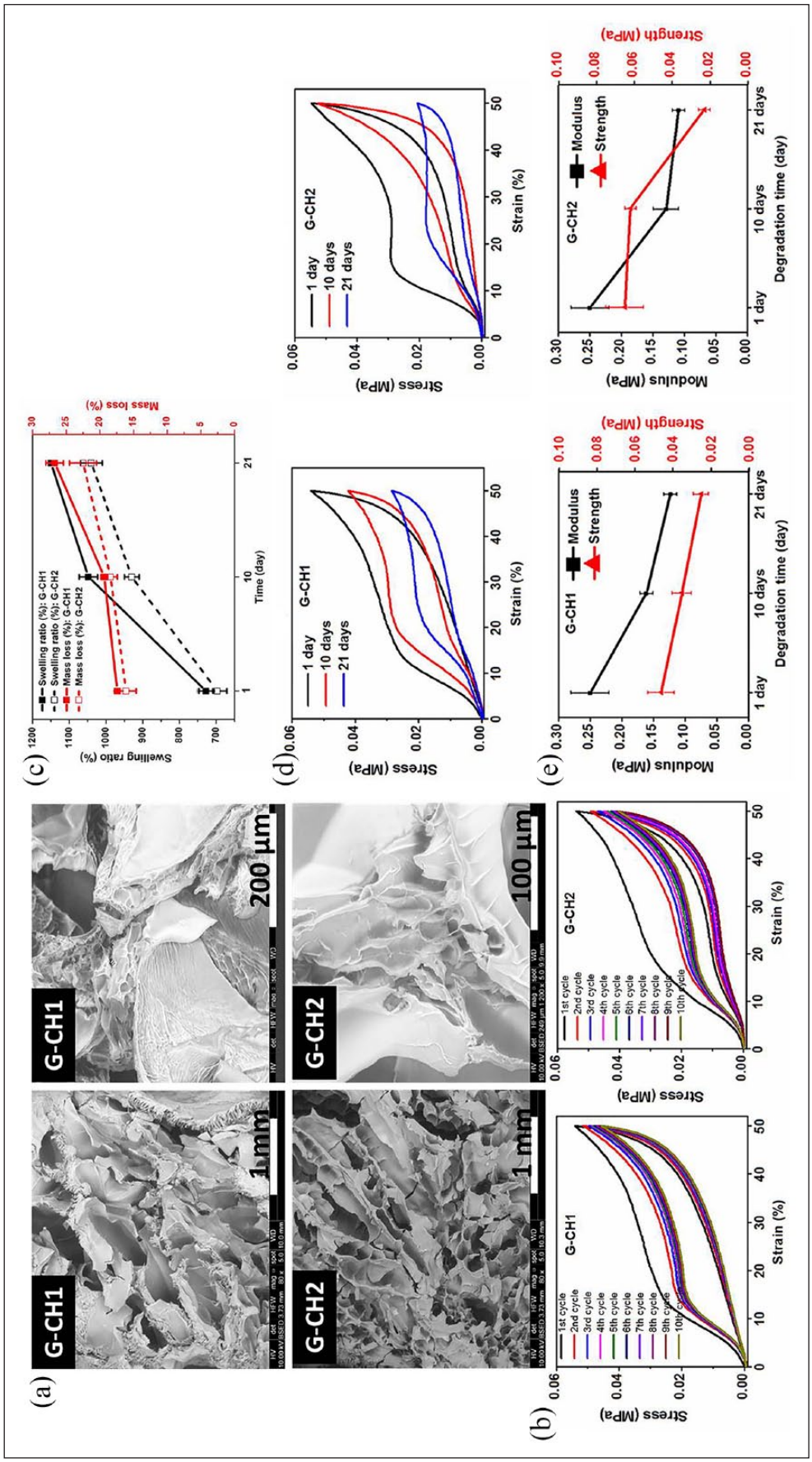

Figure 1. (a) SEM micrographs showing different magnifications of G-CH1 and G-CH2. (b) Cyclic compressive stress–strain curves of G-CH1 and G-CH2 for up to 10 consecutive cycles at 50% maximum strain. (c) Swelling ratio and mass loss trends during degradation period of G-CH1 (continuous lines) and G-CH2 (dashed lines). (d) Representative cyclic stress–strain curves obtained during degradation of hydrogels G-CH1 and G-CH2. (e) Mechanical assessment of hydrogels during degradation time of 1, 10, and 21 days: variation of modulus and strength for G-CH1, and corresponding change of modulus and strength for G-CH2.

period of 3 weeks. As expected, mass loss and swelling ratio increased over the course of experiment. Noteworthy, G, CH, and PEG as well as hydrogels originated from their grafting and crosslinking contain hydrolytically vulnerable bonds resulting in hydrolysis, breaking down the network, dissolving/leaching out the fragmented soluble fractions, and inducing mass loss, while in turn making more voids available for water and, consequently, increasing swelling ratio. Both hydrogels lost approximately 30% of their initial masses after 3 weeks. Meanwhile, swelling ratio increased by 50% and 40% of their initial values for G-CH1 and G-CH2, respectively (Figure 1(c)).

We also monitored mechanical stiffness and strength over degradation time. Representative cyclic stress–strain curves obtained during degradation of hydrogels (Figure 1(d)) demonstrated the structural and mechanical stability as well as good reversibility even after 21 days of degradation. A decreasing trend of moduli and strengths was observed over time for both hydrogels suggesting gradually breaking of cross-linked networks and consequent mass losses. The relative change of modulus and strength over the degradation period showed that hydrogels retained about 45% of their initial stiffness and strength after 3 weeks of degradation (Figure 1(e)). In addition, hydrogels lost mass during degradation time, leaving available spaces to accommodate the growing new cells and deposition of ECM.

Cells adhered well and maintained viability

BM-hMSCs and AT-hMSCs were seeded in the G-CH hydrogels and after 2 and 21 days in complete medium FBS or hPL, SEM was performed to evaluate adhesion and morphology of the cells. After 2 days, adhered cells showed a spread morphology and were anchored by filopodia to the surface of the pores within the materials. Staining of nuclei (DAPI) showed uniform distribution of the cells in the hydrogels (Figure 2(a)).

After 21 days in complete medium FBS or hPL, cells viability in the scaffolds was evaluated in three replicates using a Live/Dead assay. BM-hMSCs and AT-hMSCs in the G-CH1 and G-CH2 hydrogels were viable and distributed homogenously after 21 days of culture. Specifically, cell viability within the hydrogels ranged between 75% and 90% in all conditions, independently of the presence of either hPL or FBS, of the content of CH in the scaffold, and of cell type. No significant difference of BM-hMSCs viability were noted in both the two types of hydrogels and culture media (G-CH1 + FBS, 87.79% ± 6.80 and G-CH1 + hPL, 83.18% ± 9.41, G-CH2 + FBS, 84.75% ± 5.60 and G-CH2 + hPL, 77.75% ± 7.63) and of AT-hMSCs viability in both the two types of hydrogels and culture media (G-CH1 + FBS, 79.26% ± 16.34 and G-CH1 + hPL, 85.81% ± 9.93, G-CH2 + FBS, 82.96% ± 7.85 and G-CH2 + hPL, 84.44% ± 6.31) (Figure 2(b), Supplemental Figure S1).

G-CH1 and hPL support cell proliferation

Cell proliferation was measured by quantifying viable cells number within the G-CH hydrogels (by the CCK8 assay) at different time points after cell seeding. We found that both BM-hMSCs and AT-hMSCs proliferated over time, reaching a maximum of cell number after 21 days of culture. In particular, G-CH1 in complete medium with hPL significantly supported enhanced cell proliferation, especially for BM-hMSCs after 10 days (G-CH1 + hPL vs G-CH2 + hPL, $p = 0.0460$, G-CH1 + hPL vs G-CH1 + FBS, $p = 0.0099$, G-CH1 + hPL vs G-CH2 + FBS, $p = 0.0017$), 14 days of culture (G-CH1 + hPL vs G-CH1 + FBS, $p = 0.0270$, G-CH1 + hPL vs G-CH2 + FBS, $p < 0.0001$) and 21 days (G-CH1 + hPL vs G-CH2 + hPL, $p = 0.0105$).

Also G-CH2 in complete medium with hPL significantly supported enhanced proliferation of BM-hMSCs (G-CH2 + hPL vs G-CH2 + FBS, $p < 0.0001$).

With respect to AT-hMSCs, hPL also significantly increased cell numbers after 10 days of culture (G-CH1 + hPL vs G-CH1 + FBS, $p = 0.0406$, G-CH1 + hPL vs G-CH2 + FBS, $p = 0.0149$, G-CH2 + hPL vs G-CH2 + FBS, $p = 0.0312$) (Figure 3(a)).

Scaffolds and hPL contribute to osteogenic differentiation

Then, osteogenic differentiation of BM-hMSCs and AT-hMSCs in the G-CH1 and G-CH2 hydrogels under different culturing conditions was tested. Immunofluorescence analysis for OCN was performed and the results showed that both hMSCs types used in this study could undergo differentiation to the osteogenic lineage when seeded within the hydrogel scaffolds in differentiating conditions (Figure 3(b) and (c)). Staining for OCN after 21 days of culture revealed that in the presence of FBS no differentiation occurred independently of the scaffold or cell type if no osteogenic medium was added (Figure 3(c), GM + FBS). On the other hand, the addition of hPL significantly favored osteogenic differentiation in the absence of induction media for both scaffolds and cell types (**BM-hMSCs,** G-CH1, GM + hPL vs G-CH1, GM + FBS, $p = 0.0073$ and G-CH2, GM + hPL vs G-CH2, GM + FBS, $p = 0.0004$; **AT-hMSCs,** G-CH1, GM + hPL vs G-CH1, GM + FBS, $p < 0.0001$ and G-CH2, GM + hPL vs G-CH2, GM + FBS, $p = 0.0080$). The effect of hPL on differentiation was significantly stronger for AT than BM derived hMSCs, where, for example, for G-CH2, hPL alone allowed for a twofold increase of OCN compared to GM with FBS (**AT-hMSCs**, G-CH2, GM + hPL vs G-CH2, GM + FBS, $p = 0.0080$), and for a threefold increase in the presence of osteogenic inducers (**AT-hMSCs**, G-CH2, OM + hPL vs G-CH2, OM + FBS, $p = 0.0005$). Moreover, for G-CH1 seeded with AT-hMSCs, the effect of hPL alone allowed for a twofold increase of OCN compared to the effect of hPL in the

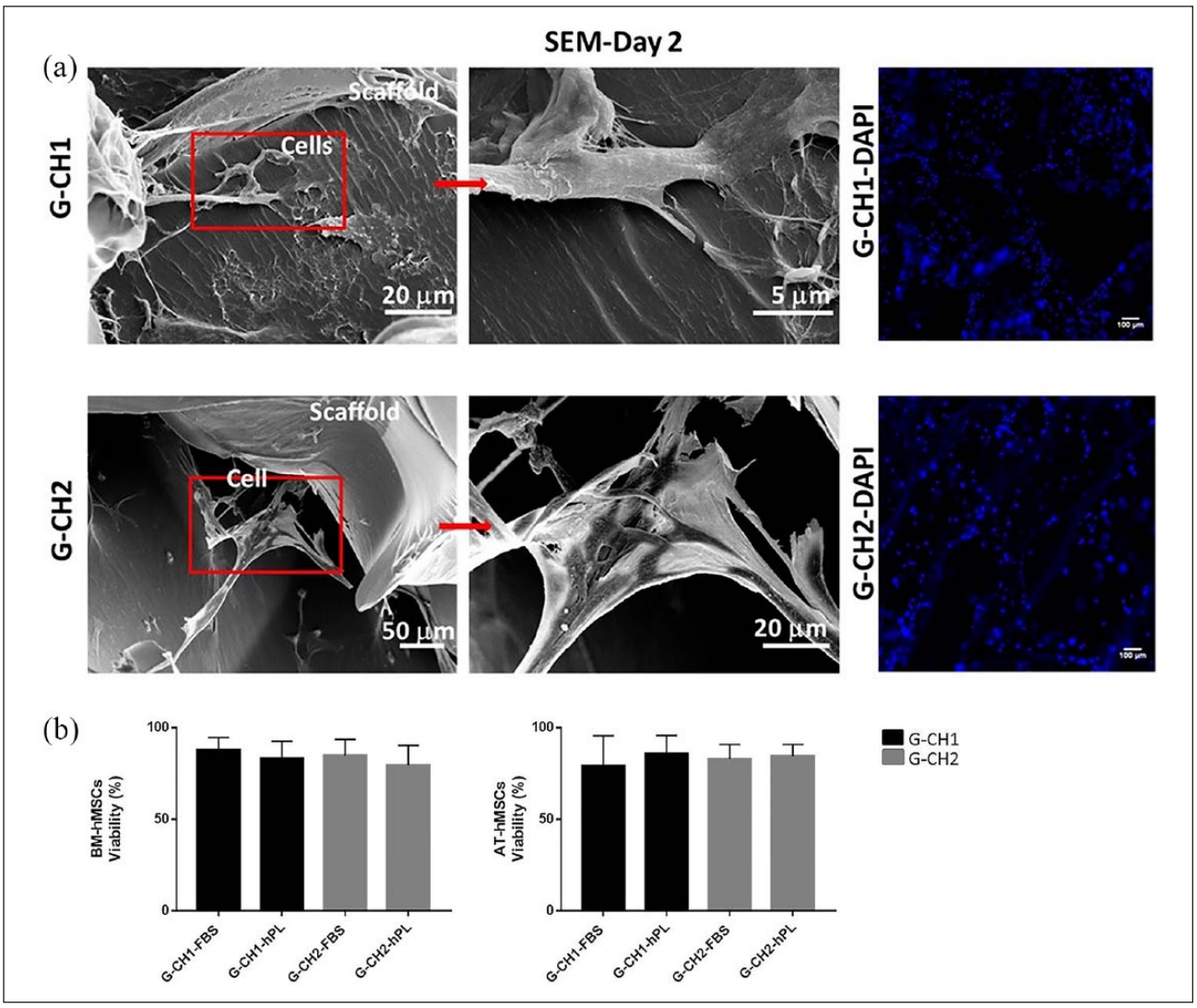

Figure 2. (a) SEM micrographs of scaffold-cells constructs at 2 days culture show morphology and adhesion of BM-hMSCs in G-CH1 scaffold and G-CH2 scaffold. SEM images are related to the midline cross sections of the scaffolds. Scale bars: 5 µm, 20 µm, and 50 µm. Corresponding staining of nuclei (DAPI) in G-CH1 scaffold **(**G-CH1-DAPI**)** and G-CH2 scaffold **(**G-CH2-DAP**)**. Scale bar: 100 µm. (b) Percentage of BM-hMSCs and AT-hMSCs viable cells cultivated for 21 days in G-CH1 and G-CH2 hydrogels in the complete medium FBS or complete medium hPL examined by live/dead staining in three replicates.

presence of osteogenic stimuli (**AT-hMSCs**, G-CH1, GM + hPL vs G-CH1, OM + hPL, $p = 0.0064$).

After 21 days, culture w/o osteogenic differentiation stimuli, the cells were still adherent and their spreading and migration into the inner regions of the scaffold were remarkable, because of the pore size and open porosity of both hydrogels (Supplemental Figure S2). SEM micrographs showed that BM-hMSCs adopted a more fully elongated and packed morphology in flattened sheet and deposited more ECM fibers in the pores of both the G-CH1 and G-CH2 hydrogels (Supplemental Figure S2). On the other hand, after 21 days of osteogenic differentiation, both scaffolds supported mineralization, as revealed by the presence of mineral deposits detected via SEM (Figure 4(a), Supplemental Figure S2).

Analysis of cell mineralization

Von Kossa staining confirmed the presence of mineralized positive area mainly localized on the scaffolds treated with OM (Figure 4(b)). SEM-EDX analysis was performed to quantify individual elements particularly focusing on calcium and phosphorus typically present in mineral deposits formed during osteogenic differentiation. EDX characterization was performed on both the G-CH hydrogels and in three distinct areas of the same sample after 21 days of osteogenic differentiation focusing on calcium and phosphorous elements. The EDX spectra associated with SEM analysis are shown in Supplemental Figure S3, from which weight and atomic ratios of elements in minerals deposited by hMSCs were determined for quantitative comparison.

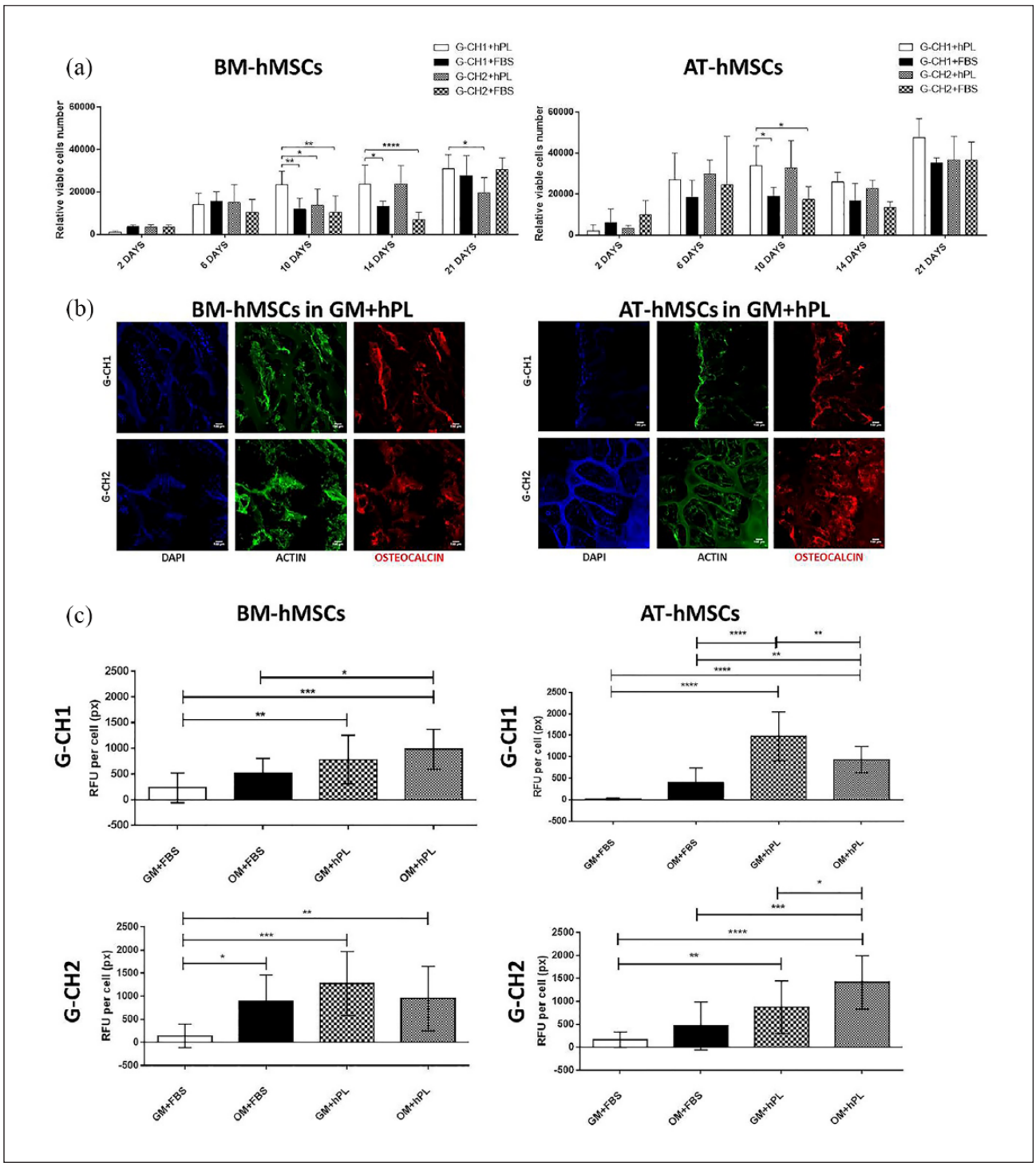

Figure 3. (a) Proliferation of BM-hMSCs and AT-hMSCs cultivated in G-CH hydrogels measured by the CCK8 assay in the complete medium FBS or complete medium hPL at different time points (2, 6, 10, 14, and 21 days). Two-way ANOVA was used for statistical analysis. Data show the average values and their significant differences (*$p \leqslant 0.05$, **$p \leqslant 0.01$, ***$p \leqslant 0.001$, ****$p \leqslant 0.0001$). (b) Pictures of immunofluorescence of OCN expression by BM-hMSCs and AT-hMSCs cultured at 21 days in G-CH1 and G-CH2 hydrogels in the complete medium hPL (GM + hPL). Scale bar: 100 µm. (c) Graphs of immunofluorescence analysis of OCN expression by BM-hMSCs and AT-hMSCs cultured at 21 days in G-CH1 and G-CH2 hydrogels in the complete medium FBS (GM + FBS) or complete medium hPL (GM + hPL) or osteogenic medium FBS (OM + FBS) or osteogenic medium hPL (OM + hPL). One-way ANOVA was used for statistical analysis of the fluorescence intensity on BM-hMSCs and AT-hMSCs cultured at 21 days in G-CH1 and G-CH2 hydrogels.

Data show the average values and their significant differences (*$p \leqslant 0.05$, **$p \leqslant 0.01$, ***$p \leqslant 0.001$, ****$p \leqslant 0.0001$).

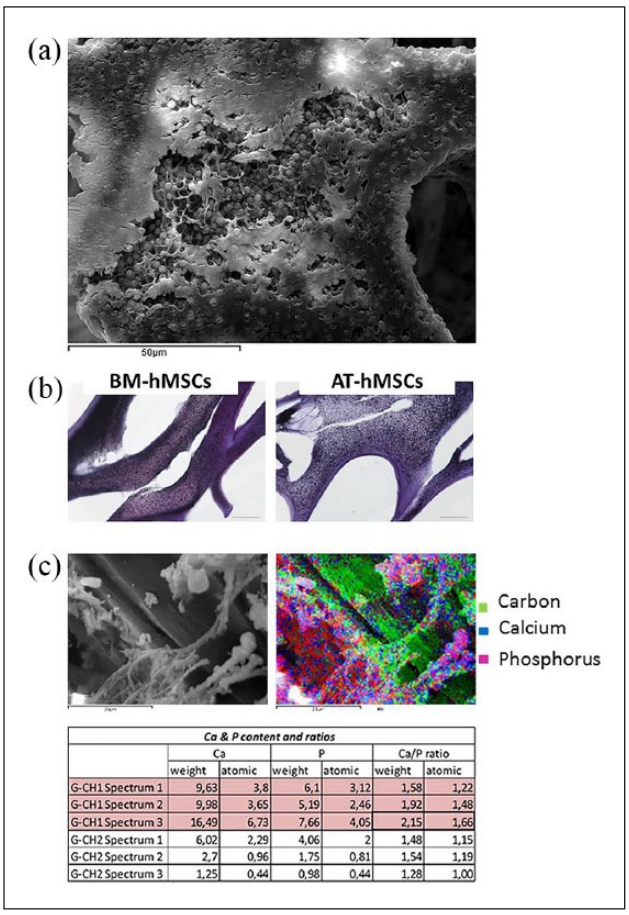

Ca & P content and ratios						
	Ca		P		Ca/P ratio	
	weight	atomic	weight	atomic	weight	atomic
G-CH1 Spectrum 1	9,63	3,8	6,1	3,12	1,58	1,22
G-CH1 Spectrum 2	9,98	3,65	5,19	2,46	1,92	1,48
G-CH1 Spectrum 3	16,49	6,73	7,66	4,05	2,15	1,66
G-CH2 Spectrum 1	6,02	2,29	4,06	2	1,48	1,15
G-CH2 Spectrum 2	2,7	0,96	1,75	0,81	1,54	1,19
G-CH2 Spectrum 3	1,25	0,44	0,98	0,44	1,28	1,00

Figure 4. (a) SEM micrographs of calcium phosphate deposition in G-CH1 with BM-hMSCs in OM with hPL at day 21. Scale bar: 50 µm. (b) Von Kossa staining of BM-hMSCs and AT-hMSCs on G-CH1 scaffold in OM with hPL at day 21. Bars = 50µm. (c) The image refers to the evaluation of calcium phosphate deposition with SEM-EDX of G-CH1 with BM-hMSCs in OM with hPL at day 21. The area of the colored element map on the right corresponds to the sample area on the SEM image on the left hand side. The table refers to calcium and phosphorus ratios in G-CH1 and G-CH2 with BM-hMSCs in OM with hPL (three spectra taken in different areas of the sample for each condition) at day 21.

EDX analysis of the constructs showed evidence of calcium phosphate crystals, a sign of mineralized matrix (Ca:P in distinct areas Supplemental Figure S3), when cells were cultured in OM with hPL. On the other hand, no calcium phosphates were observed after culture in complete medium hPL (Supplemental Figure S3). Furthermore, the Ca/P weight and atomic ratios in G-CH1 and G-CH2 were between 1.5 and 2.0 and close to that of bone, whose mineral primarily consists of Ca and P with a Ca/P ratio from 1.4–1.7.[30] As shown in the table, on G-CH1 Ca/P weight and atomic ratios (1.58/1.22; 1.92/1.48; 2.15/1.66) were closer to the hydroxyapatite (HA; 2.22/1.66) and tricalcium phosphate (2.0/1.5) ones compared to G-CH2 (1.48/1.15; 1.54/1.19; 1.28/1.00) (Figure 4(c)). These results suggest that our G-CH hydrogel systems were able to mimic the physiological environment showing mineralization already detectable at day 21 using OM with hPL, but not using hPL alone.

Proteomic characterization of hPL and PPP highlight factors involved in cell stimulating effects

About 500 different protein IDs were identified in hPL (n = 501) and PPP (n = 491), respectively, considering both not depleted and depleted samples (Figure 5(a)). An increase in identification power was noticed in depleted plasma derivatives with respect to their non depleted counterpart, ranging from 15% to 21%.

In the depleted specimens, about 40% (169 IDs) of the proteins detected in hPL were not observed in the PPP, while in not depleted samples 36% (130 IDs) were present only in hPL (Figure 5(a)). In particular, combining the lists of protein IDs in different sample groups, 59 were uniquely present in hPL and not in common with PPP independently from the depletion process (Figure 5(b)). The related enriched biological processes and KEGG pathways, of these 59 proteins, were obtained using STRING[26] and are listed in Supplemental Table 1 and in Supplemental Figure S4. Interestingly, the majority of the 59 molecules are implicated in stress response and wound healing (56% and 46% of all proteins present in the panel, respectively), platelet and cell activation (36% and 41%, respectively), cell differentiation (31%) and cell adhesion (29%) (Supplemental Table 1). It has been also observed that some of the proteins specific of hPL are involved in several pathways that are likely to be strictly linked the promotion of repair mechanisms, such as signal transduction (as RAP-1 and HIF-1 signaling pathway), cell adhesion and motility, and carbohydrate metabolisms (Supplemental Figure S4). The more critical nodes in the related networks, moreover, are represented by key proteins typical of the platelet degranulation (as ACTN1, TLN-1, PF4, VCL, MMRN1, ITGA2B, and ITGB3), neutrophil degranulation (as RAP1B), cell-matrix interaction (as PXN, ITGB1, ILX), and also osteoblast differentiation and bone development (as TPM4 and SPARC) (Supplemental Figure S4).

In addition to those proteins identified exclusively in hPL, label-free relative quantification pinpointed 7 (Supplemental Figure S5) and 23 (Supplemental Figure S6) proteins significantly altered in their abundances comparing hPL vs PPP in not depleted and in depleted samples, respectively (fold change ≥ 1.5; $p < 0.05$; ≥ 2 unique peptides; in at least 4 replicates). Three of these differences were in common and up-represented in hPL, including platelet basic protein, a factor known to be involved in the regulation of cell proliferation and observed to be more than 20 fold more concentrated in hPL vs PPP both in depleted and not depleted samples. Enrichment of the biological processes and networks that

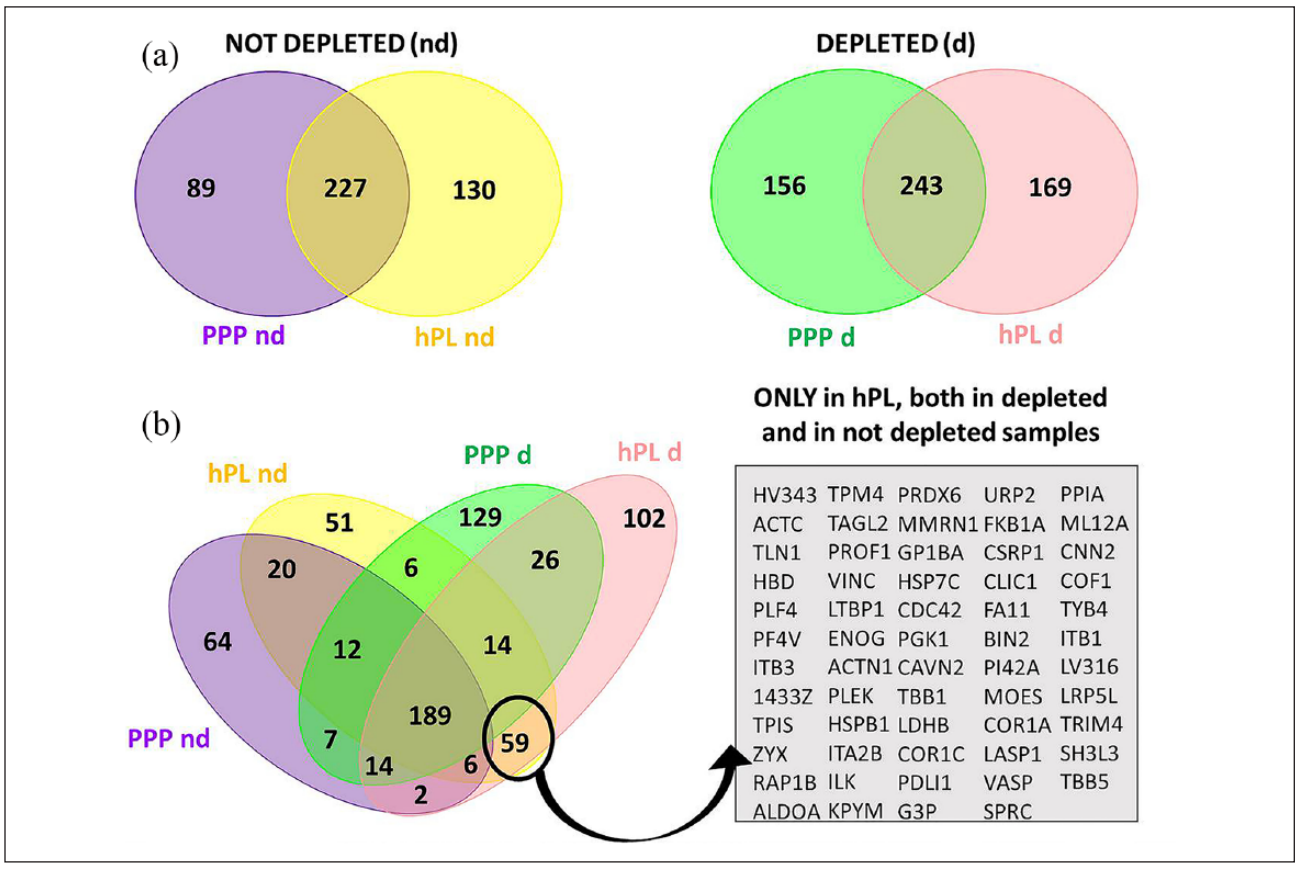

Figure 5. (a) Venn diagram of identified proteins in hPL and PPP in depleted and not depleted samples. (b) Overlap between list of proteins identified in hPL and PPP highlight a panel of 59 proteins specific of hPL independently of sample preparation method.

involve de-regulated proteins in hPL compared to PPP for both depleted and not depleted samples are illustrated in Supplemental Figure S7.

Discussion

Tissue engineering using biomaterials or scaffolds as temporary matrices for hMSCs proliferation and osteochondral differentiation is a promising strategy for tissue repair of bone or cartilage. Using a freeze-drying and post-curing technique, two biocompatible CH-G hybrid hydrogels with different CH content, G-CH1 (8.1%) and G-CH2 (14.9%), were developed, with the aim to produce scaffolds with mechanical and functional properties adequate for bone repair (Figure 1).

Scaffold stiffness is a relevant property for cell proliferation, osteogenic differentiation, and for the maintenance of structural integrity during biodegradation. The hydrogels obtained using this simple and solvent/additive free preparation technique, showed improved structural and physicomechanical properties compared to literature.[9,31,32] They showed suitable structural stability, good swellability, porosity adequate to the cell size and high pore interconnectivity. Increasing amount of CH into the G-CH network reduced the stiffness and strength leading to a softer material (Table 1). Both hydrogels exhibited viscoelastic behavior, they maintained their original shape and showed no sign of mechanical failure under compressive loading–unloading cycles at relatively high deformation level (Figure 1(b)). During hydrolytic degradation, after 3 weeks, hydrogels retained their structural stability and elasticity, while stiffness and strength were reduced to half of their initial values (Figure 1(e)). Moreover, during degradation, both hydrogels lost approximately 30% of their initial masses after 3 weeks, while swelling ratio increased leaving spaces available to allow the growth of new cells and the deposition of ECM (Figure 1(c)). Thus, physicomechanical properties and CH content can be modulated by this preparation process developed ad hoc to obtain high performance systems and in turn to adapt the scaffolds to the potential use in vivo.

CH is a biocompatible, biodegradable material with intrinsic antibacterial activity that we used in this study to favor adhesion, proliferation, and bone formation of BM/AT-hMSCs.[33–37] Many efforts have been attempted to better support these cell functions, by adding or incorporating CH with other components, such as glycerol phosphate, poly-*N*-isopropylacrylamide, lactide, poly-ethylene oxide,

or nano-particles.[38,39] However, these studies did show neither a clear advantage of a specific combination of biomaterials nor a definition of the optimal concentration of CH in these hydrogel systems.

High interconnectivity and optimal porosity of both produced scaffolds allowed cell colonization of the entire structure even in static conditions without the use of a bioreactor (Figure 2). These characteristics were not fully matched in other hydrogel systems and the cell infiltration procedure was optimized using a cold static seeding method instead of the "classic" static seeding method at 37°C.[27,40,41]

With attention to potential clinical translatability, appropriate porosity and interconnectivity are known to be important features, because they allow not only the optimal adhesion and proliferation of MSCs but also transportation of nutrients and the interaction of cells with glycosaminoglycans, proteoglycans, cytokines, and GFs.[42] It is known from laboratory practice that during the initial seeding phase, a part of the cells leaves the scaffold and they adhere to the culture well. Therefore, we moved the samples to new culture plates after a short incubation time. Consequently, proliferation results from CCK8 assay show that the number of cells proliferating after 2 days was lower compared to the number of cells added during the initial seeding phase (Figure 3(a)). However, proliferation was considerable from day 2 to day 6 of culture, in accordance with previous studies.[43–46] Interestingly, AT-hMSCs grew exponentially until reaching a plateau-phase after 10 days, which was possibly followed by cell death after 14 days. Then, cells resumed their growth and their number increased again after 21 days. This was not observed in BM-hMSCs, where an earlier onset of the osteogenic differentiation could be expected in comparison to AT-hMSCs (Figure 3(c)), limiting their proliferative potential. Hence, BM-derived cells proliferated more slowly and didn't experience such a decrease in cell numbers after an initial exponential growth.

As confirmed by the viability assay, all the cells anchored to the surface of the hydrogels were viable and proliferating as desired. Particularly, no significant difference of BM-AT-hMSCs viability was observed in the two types of hydrogels with FBS or hPL. In all, 80%–90% of BM-AT-hMSCs were viable, suggesting that there was no significant limitation in the nutrient supply in all the conditions (Figure 2(b), Supplemental Figure S1).

The cell culture procedures were performed with FBS in comparison with hPL, and we found that hPL was not only able to stimulate cell growth and proliferation but also osteo-differentiation of BM/AT-hMSCs per se. Results from immunostaining analysis showed that BM-hMSCs and AT-hMSCs cultured in both the G-CH hybrid hydrogels were efficiently induced to differentiate toward the osteogenic lineage not only in the presence of osteogenic inducers but also using hPL alone in the absence of osteo-inductive media for both scaffolds and cell types and after 3 weeks of culture (Figure 3(b) and (c)). Interestingly, even if the differentiation levels of both cell types are similar, hPL has a stronger osteogenic effect on AT-derived cells compared to BM-derived cells. Indeed, AT-hMSCs have a lower level of osteogenic phenotype in GM with FBS compared to BM-hMSCs. This could be explained by a possible specific effect of the particular 3D environment, especially the G-CH1 hydrogel that preserves stemness of the AT-derived cells when no hPL or osteostimulants are added. Upon their addition, there is a two or even threefold increase in OCN levels. A role can also be played by the different source of these cells and their predisposition to differentiate into different lineages with different efficacy.[47]

Our data are in line with previous literature where platelet GF cocktail was used for the ex-vivo expansion of hMSCs, showing significantly better results compared to previous strategies where a single GF was used.[48–52] To better understand the positive effects of hPL through stimulation of multiple signaling pathways, we then investigated the proteomic composition of hPL by label-free nLC-MS/MS. Shotgun analysis and label-free quantification of hPL and PPP allowed to "proteomically" characterize the supplement and to highlight possible candidates responsible for the beneficial effects on the MSCs proliferation and osteo-genic differentiation. In all, 59 proteins were exclusively present in hPL and not in PPP independently from the sample processing methods (Figure 5(b)), whereas 7 and 23 proteins were observed significantly altered in their abundances when comparing hPL vs PPP in not depleted and in depleted samples, respectively (Supplemental Figure S5, Supplemental Figure S6). This specificity suggests that the list of these proteins (85 different IDs in total) could represent a possible panel of factors involved in cell stimulating effect of this supplement. In particular, CXCL7 (platelet basic protein-PPBP) a positive regulator of cell proliferation was found strongly up-represented in hPL both in depleted and not depleted samples (ratio >20). Functional annotation tools allowed to highlight the biological processes, pathways, and networks enriched in these panels of proteins specific of hPL, not present or less concentrated in PPP (Supplemental Figure S4, Supplemental Figure S6, Supplemental Table 1). Most of these functional signatures relate to platelet degranulation, wound healing, and cell adhesion, but an involvement of other several specialized functions related with the cellular repairing mechanisms and the regulation of cell differentiation was also observed, suggesting a high complexity of the molecular scenario. It also cannot be excluded that the positive proliferation and differentiation effects of hPL per se could be influenced by the interaction of hPL with the G-CH hydrogel constituents.

Indeed, we found that G-CH hydrogels, particularly G-CH1, in presence of complete medium hPL, have a great potential in terms of supporting BM-hMSC and AT-hMSC proliferation and guide them to differentiate toward the osteogenic lineage.

To further investigate the ability of our G-CH hydrogel systems to mimic the physiological environment and support bone regeneration, elemental analysis was performed and the results showed that the mineralization process was already detectable at day 21 in the presence of osteogenic medium hPL but not using hPL alone. While results from staining for the osteogenic marker OCN showed that hPL alone induces osteogenic differentiation of cells, there is no evidence of mineralization in complete medium with hPL after 21 days of culture from SEM/EDX analysis (Supplemental Figure S3). Early mineralization is only detected after adding osteogenic stimuli in the culture medium. Further analyses after four or more weeks of culture are then needed to investigate the mineralization processes supported by hPL in the absence of induction media. In fact, generally 3 weeks are necessary to lead hMSCs toward the osteogenic differentiation while almost 4 weeks or more are required for mineralization to occur.[53–55]

Inorganic phosphates on cell surface detected via SEM could be deemed as prime evidence for osteo-genic differentiation of hMSCs and this deposition of calcium phosphate was crucial to scaffold mineralization processes (Supplemental Figure S2). The Ca/P weight and atomic ratios supported the presence of HA, suggesting a marked ability of the G-CH hydrogels to mimic the physiological environment. Interestingly, G-CH1 characterized by less content of CH was more advantageous for cell growth and scaffold mineralization. Indeed, G-CH1 supported a significantly higher cell proliferation, particularly for BM-hMSCs (Figure 3(a)), as well as a better cell differentiation, confirmed via Von Kossa staining showing mineralization (Figure 4(b)).

In summary, our results demonstrated that both G-CH1 and G-CH2 synthetic hydrogel scaffolds are biocompatible and bioresorbable and their chemical, morphological, and mechanical properties are suitable to support cells growth, osteo-differentiation, and mineralization, and their potential application for bone regeneration. Moreover, we show that a cell culture procedure using hPL instead of FBS, besides avoiding the risks of transmitting animal diseases, contains crucial mitogenic and chemotactic molecules that promote cell differentiation and tissue repair. Hence, these scaffolds in combination with hPL have the potential to provide a clinical grade biomedical device. hPL has the potential to become the gold standard supplement for hMSC propagation in regenerative medicine, in addition to already commercialized products,[18,19,56,57] even if a standardization of protocols has to be investigated yet.

Acknowledgements

The authors are highly grateful to the Brescia section of Associazione Donatrici Italiane Sangue Cordone Ombelicale (ADISCO) for supporting the research with hemopoietic and mesenchymal stem cells and Sterigenics Italy (Bologna, Italy) for sterilizing the materials.

Declaration of conflicting interests

The author(s) declared no potential conflicts of interest with respect to the research, authorship, and/or publication of this article.

Funding

The author(s) disclosed receipt of the following financial support for the research, authorship, and/or publication of this article: The work was funded by Brescia University Health & Wealth Research Program, Fondazione Comunità Bresciana, European Research Council (ERC—HealInSynergy 306990), EPSRC (EP/P001114/1) and MRC (MR/S005412/1). This work was also funded by a grant from the UK Regenerative Medicine Platform.

ORCID iDs

Federica Re https://orcid.org/0000-0003-4219-8695
Vladimira Moulisova https://orcid.org/0000-0003-0700-2837
Corrado Paganelli https://orcid.org/0000-0003-1085-3587
Manuel Salmeron-Sanchez https://orcid.org/0000-0002-8112-2100

Supplemental material

Supplemental material for this article is available online.

References

1. Patrick Jr CW, Mikos AG and McIntire LV. Prospectus of tissue engineering. In: Patrick CW, Mikos AG and McIntire LV (eds) *Frontiers in tissue engineering*. 1st ed. New York: Elsevier, 1998, pp. 3-14.
2. Lutolf MP and Hubbell JA. Synthetic biomaterials as instructive extracellular microenvironments for morphogenesis in tissue engineering. *Nat Biotechnol* 2005; 23(1): 47–55.
3. Hutson CB, Nichol JW, Aubin H, et al. Synthesis and characterization of tunable poly(ethylene glycol): gelatin methacrylate composite hydrogels. *Tissue Eng Part A* 2011; 17(13–14): 1713–1723.
4. Fisher OZ, Khademhosseini A, Langer R, et al. Bioinspired materials for controlling stem cell fate. *Acc Chem Res* 2010; 43(3): 419–428.
5. Rehfeldt F, Engler AJ, Eckhardt A, et al. Cell responses to the mechanochemical microenvironment—implications for regenerative medicine and drug delivery. *Adv Drug Deliv Rev* 2007; 59(13): 1329–1339.
6. Engler AJ, Sen S, Sweeney HL, et al. Matrix elasticity directs stem cell lineage specification. *Cell* 2006; 126(4): 677–689.
7. Sionkowska A. Current research on the blends of natural and synthetic polymers as new biomaterials: review. *Prog Polym Sci* 2011; 36: 1254–1276.
8. Perez RA, Won JE, Knowles JC, et al. Naturally and synthetic smart composite biomaterials for tissue regeneration. *Adv Drug Deliv Rev* 2013; 65(4): 471–496.
9. Klotz BJ, Gawlitta D, Rosenberg AJWP, et al. Gelatin-methacryloyl hydrogels: towards biofabrication-based tissue repair. *Trends Biotechnol* 2016; 34(5): 394–407.
10. Saraiva SM, Miguel SP, Ribeiro MP, et al. Synthesis and characterization of a photocrosslinkable chitosan-gelatin hydrogel aimed for tissue regeneration. *RSC Adv* 2015; 5: 63478–63488.

11. Lopez-Perez PM, Da Silva RMP, Serra C, et al. Surface phosphorylation of chitosan significantly improves osteoblast cell viability, attachment and proliferation. *J Mater Chem* 2010; 20: 483–491.
12. Wu T, Liu Y, Wang B, et al. The roles of mesenchymal stem cells in tissue repair and disease modification. *Curr Stem Cell Res Ther* 2014; 9(5): 424–431.
13. Si YL, Zhao YL, Hao HJ, et al. MSCs: biological characteristics, clinical applications and their outstanding concerns. *Ageing Res Rev* 2011; 10(1): 93–103.
14. Dominici M, Le Blanc K, Mueller I, et al. Minimal criteria for defining multipotent mesenchymal stromal cells. *Cytotherapy* 2006; 8(4): 315–317.
15. Re F, Perucca S, Bernardi S, et al. Development of a 3D cell culture model based on biocompatible polymeric scaffolds engineered with human mesenchymal stromal cells (MSCs) for skin, cartilage and bone regenerative therapy. In: *Proceedings of the international translational and regenerative medicine conference*, Rome, 25–27 April 2018.
16. Re F, Perucca S, Sartore L, et al. Development of a cell culture model based on biocompatible polymeric scaffolds engineered with human mesenchymal stromal cells (MSCs) for cartilage and bone regenerative therapy. In: *Proceedings of the 44th annual meeting of the European society for blood and marrow transplantation*, Lisbon, 18–21 March 2018.
17. Doucet C, Ernou I, Zhang Y, et al. Platelet lysates promote mesenchymal stem cell expansion: a safety substitute for animal serum in cell-based therapy applications. *J Cell Physiol* 2005; 205(2): 228–236.
18. Muraglia A, Todeschi MR, Papait A, et al. Combined platelet and plasma derivatives enhance proliferation of stem/progenitor cells maintaining their differentiation potential. *Cytotherapy* 2015; 17(12): 1793–1806.
19. Spano R, Muraglia A, Todeschi MR, et al. Platelet-rich plasma-based bioactive membrane as a new advanced wound care tool. *J Tissue Eng Regen Med* 2018; 12(1): e82–e96.
20. Han T, Wang H and Zhang YQ. Combining platelet-rich plasma and tissue-engineered skin in the treatment of large skin wound. *J Craniofac Surg* 2012; 23(2): 439–447.
21. Chinello C, Stella M, Piga I, et al. Proteomics of liquid biopsies: Depicting RCC infiltration into the renal vein by MS analysis of urine and plasma. *J Proteomics* 2018; 191: 29–37.
22. Chinello C, Cazzaniga M, DeSio G, et al. Tumor size, stage and grade alterations of urinary peptidome in RCC. *J Transl Med* 2015; 13: 332.
23. Liu X, Chinello C, Musante L, et al. Intraluminal proteome and peptidome of human urinary extracellular vesicles. *Proteomics Clin Appl* 2015; 9(5–6): 568–573.
24. Zhang J, Xin L, Shan B, et al. PEAKS DB: de novo sequencing assisted database search for sensitive and accurate peptide identification. *Mol Cell Proteomics* 2012; 11(4): 010587.
25. Jensen LJ, Kuhn M, Stark M, et al. STRING 8—a global view on proteins and their functional interactions in 630 organisms. *Nucleic Acids Res* 2009; 37: D412–D416.
26. STRING. STRING: functional protein association networks (2018, version 10.5), http://www.string-db.org
27. Mehr NG, Li X, Chen G, et al. Pore size and LbL chitosan coating influence mesenchymal stem cell in vitro fibrosis and biomineralization in 3D porous poly(epsilon-caprolactone) scaffolds. *J Biomed Mater Res A* 2015; 103(7): 2449–2459.
28. Diani J, Fayolle B and Gilormini P. A review on the Mullins effect. *Eur Polym J* 2009; 45: 601–612.
29. Dey K, Agnelli S, Serzanti M, et al. Preparation and properties of high performance gelatin-based hydrogels with chitosan or hydroxyethyl cellulose for tissue engineering applications. *Int J Polym Mater Po* 2019; 68: 183–192.
30. Fernandez JM, Molinuevo MS, Cortizo MS, et al. Development of an osteoconductive PCL-PDIPF-hydroxyapatite composite scaffold for bone tissue engineering. *J Tissue Eng Regen Med* 2011; 5(6): e126–e135.
31. Dey K, Agnelli S and Sartore L. Dynamic freedom: substrate stress relaxation stimulates cell responses. *Biomater Sci* 2019; 7: 836–842.
32. Kang H, Shih YRV, Hwang Y, et al. 2014. Mineralized gelatin methacrylate-based matrices induce osteogenic differentiation of human induced pluripotent stem cells. *Acta Biomaterialia* 2014; 10: 4961–4970.
33. Aimin C, Chunlin H, Juliang B, et al. Antibiotic loaded chitosan bar. *Clin Orthop Relat Res* 1999; 366: 239–247.
34. Seol YJ, Lee JY, Park YJ, et al. Chitosan sponges as tissue engineering scaffolds for bone formation. *Biotechnol Lett* 2004; 26(13): 1037–1041.
35. Dai T, Tanaka M, Huang YY, et al. Chitosan preparations for wounds and burns: antimicrobial and wound-healing effects. *Expert Rev Anti Infect Ther* 2011; 9(7): 857–879.
36. Zhao F, Grayson WL, Ma T, et al. Effects of hydroxyapatite in 3-D chitosan-gelatin polymer network on human mesenchymal stem cell construct development. *Biomaterials* 2006; 27(9): 1859–1867.
37. Breyner NM, Hell RC, Carvalho LR, et al. Effect of a three-dimensional chitosan porous scaffold on the differentiation of mesenchymal stem cells into chondrocytes. *Biomaterials* 2005; 26: 5983–5990.
38. Levengood SL and Zhang M. Chitosan-based scaffolds for bone tissue engineering. *J Mater Chem B* 2014; 2: 3161–3184.
39. Mekhail M and Tabrizian M. Injectable chitosan-based scaffolds in regenerative medicine and their clinical translatability. *Adv Healthc Mater* 2014; 3(10): 1529–1545.
40. Nandi SK, Kundu B and Basu D. Protein growth factors loaded highly porous chitosan scaffold: a comparison of bone healing properties. *Mater Sci Eng C Mater Biol Appl* 2013; 33(3): 1267–1275.
41. Petrie Aronin CE, Sadik KW, Lay AL, et al. Comparative effects of scaffold pore size, pore volume, and total void volume on cranial bone healing patterns using microsphere-based scaffolds. *J Biomed Mater Res A* 2009; 89(3): 632–641.
42. Danilchenko SN, Kalinkevich OV, Pogorelov MV, et al. Characterization and in vivo evaluation of chitosan-hydroxyapatite bone scaffolds made by one step coprecipitation method. *J Biomed Mater Res A* 2011; 96(4): 639–647.
43. Cruz DM, Gomes M, Reis RL, et al. Differentiation of mesenchymal stem cells in chitosan scaffolds with double micro and macroporosity. *J Biomed Mater Res A* 2010; 95(4): 1182–1193.
44. Steiner D, Lingens L, Fischer L, et al. Encapsulation of mesenchymal stem cells in chitosan/β-glycerophosphate

hydrogel for seeding on a novel calcium phosphate cement scaffold. *Med Eng Phys* 2018; 56: 9–15.
45. Dong L, Wang SJ, Zhao XR, et al. 3D-printed poly(ε-caprolactone) scaffold integrated with cell-laden chitosan hydrogels for bone tissue engineering. *Sci Rep* 2017; 7: 13412.
46. Gu Y, Bai Y and Zhang D. Osteogenic stimulation of human dental pulp stem cells with a novel gelatin-hydroxyapatite-tricalcium phosphate scaffold. *J Biomed Mater Res A* 2018; 106(7): 1851–1861.
47. Pizzute T, Lynch K and Pei M. Impact of tissue-specific stem cells on lineage-specific differentiation: a focus on the musculoskeletal system. *Stem Cells Rev* 2016; 11: 119–132.
48. Chevallier N, Anagnostou F, Zilber S, et al. Osteoblastic differentiation of human mesenchymal stem cells with platelet lysate. *Biomaterials* 2010; 31(2): 270–278.
49. Xie X, Wang Y, Zhao C, et al. Comparative evaluation of MSCs from bone marrow and adipose tissue seeded in PRP-derived scaffold for cartilage regeneration. *Biomaterials* 2012; 33(29): 7008–7018.
50. Leotot J, Coquelin L, Bodivit G, et al. Platelet lysate coating on scaffolds directly and indirectly enhances cell migration, improving bone and blood vessel formation. *Acta Biomater* 2013; 9(5): 6630–6640.
51. Oryan A, Alidadi S, Bigham-Sadegh A, et al. Effectiveness of tissue engineered chitosan-gelatin composite scaffold loaded with human platelet gel in regeneration of critical sized radial bone defect in rat. *J Control Release* 2017; 254: 65–74.
52. Dallari D, Fini M, Stagni C, et al. In vivo study on the healing of bone defects treated with bone marrow stromal cells, platelet-rich plasma, and freeze-dried bone allografts, alone and in combination. *J Orthop Res* 2016; 24: 877–888.
53. Yorukoglu AC, Kiter AE, Akkaya S, et al. A concise review on the use of mesenchymal stem cells in cell sheet-based tissue engineering with special emphasis on bone tissue regeneration. *Stem Cells Int* 2017; 2017: 2374161.
54. Thimm BW, Wechsler O, Bohner M, et al. In vitro ceramic scaffold mineralization: comparison between histological and micro-computed tomographical analysis. *Ann Biomed Eng* 2013; 41(12): 2666–2675.
55. Weisgerber DW, Caliari SR and Harley BA. Mineralized collagen scaffolds induce hMSC osteogenesis and matrix remodeling. *Biomater Sci* 2015; 3(3): 533–542.
56. Muraglia A, Ottonello C, Spano R, et al. Biological activity of a standardized freeze-dried platelet derivative to be used as cell culture medium supplement. *Platelets* 2014; 25(3): 211–220.
57. Muraglia A, Nguyen VT, Nardini M, et al. Culture medium supplements derived from human platelet and plasma: cell commitment and proliferation support. *Front Bioeng Biotechnol* 2017; 5: 66.